JOURNAL OF CHEMICAL INFORMATION AND MODELING

Article

pubs.acs.org/jcim

Pharmacophore Model for Wnt/Porcupine Inhibitors and Its Use in Drug Design

Anders Poulsen,* Soo Yei Ho, Weiling Wang, Jenefer Alam, Duraiswamy A. Jeyaraj, Shi Hua Ang, Eldwin Sum Wai Tan, Grace Ruiting Lin, Vivien Wei Wen Cheong, Zhiyuan Ke, May Ann Lee, and Thomas H. Keller

Experimental Therapeutics Centre, Agency for Science, Technology and Research, 31 Biopolis Way, Nanos Level 3, Singapore 138669

Supporting Information

ABSTRACT: Porcupine is a component of the Wnt pathway which regulates cell proliferation, migration, stem cell self-renewal, and differentiation. The Wnt pathway has been shown to be dysregulated in a variety of cancers. Porcupine is a membrane bound *O*-acyltransferase that palmitoylates Wnt. Inhibiting porcupine blocks the secretion of Wnt and effectively inhibits the Wnt pathway. Using high throughput screening, we have identified a number of novel porcupine inhibitors with diverse scaffolds. The pharmacophore requirements for our porcupine inhibitors were elucidated, and a pharmacophore model is proposed. Our compounds as well as all currently published porcupine inhibitors may be fitted to this model in low energy conformations with good superimposition of the pharmacophore elements. The model also explains the stereochemical requirements of our chiral porcupine inhibitors. The pharmacophore model was successfully used for designing 3 new series of porcupine inhibitors having a tricyclic xantine, a phtalimide, or a piperidine−maleimide scaffold.

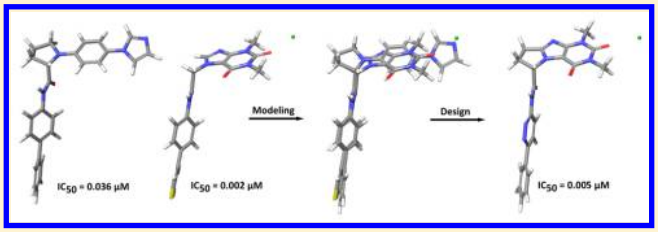

1. INTRODUCTION

Wingless-type (Wnt) signaling is essential for embryonic development and plays a critical role in regulating stem cell proliferation and differentiation in the adult organism. Wnt signaling is involved in diverse processes such as bone metabolism, atherosclerosis, angiogenesis, acute renal failure, and neurodegenerative diseases.[1] Canonical Wnt signaling is dysregulated in multiple cancers. This may be due to the mutation of major components of the Wnt signaling pathway such as adenomatous polyposis coli and β-catenin,[2−4] silencing of genes that encode for inhibitory Wnt ligands such as secreted frizzled-related proteins and Dickkopf-related proteins[5−7] or overexpression of Wnt proteins such as frizzleds and dishevelled.[8,9] Overexpression of Wnt has been implicated in the process of tumorigenesis and metastasis.[10] Inhibitors of Wnt secretion would reduce the expression of Wnt and may have an effect on inhibiting tumor growth. A promising way of blocking Wnt secretion is through the inhibition of the Wnt-acyltransferase porcupine.[11] Porcupine adds palmitoleate to a serine residue in Wnt which is required for the secretion of Wnts.[12−14] Compounds targeting porcupine have been found in a high throughput screen done by Chen et al.[15] C59, an inhibitor of porcupine, has been shown to inhibit the growth of Wnt-driven mammary cancer in mice.[11] More recently, it was reported that a porcupine inhibitor in Phase I clinical trial, LGK974, inhibits head and neck cancer and pancreatic ductal adenocarcinoma cell lines and mouse xenograft models.[16,17]

Consequently, we did a high throughput screen against porcupine with the aim of finding Wnt pathway inhibitors. A number of potent inhibitors were discovered, and hit validation in secondary assays confirmed these to be porcupine inhibitors [Supporting Information]. This article describes the pharmacophore preferences of our own and those of previously published porcupine, as well as the putative bioactive conformation of these compounds.

2. COMPUTATIONAL METHODS

2.1. Conformational Search, Force Fields, and Solvation Model. The molecules were built using Maestro 9.0.[18] The conformational space was searched using the Monte Carlo (MCMM) method[19] as implemented in MacroModel version 9.7.[18] All heavy atoms and hydrogens on heteroatoms were included in the test for duplicate conformations. All rotatable single bonds were included in the conformational search, and all aliphatic rings were ring-opened, and quaternary atoms were allowed to invert. The amide holding the amide donor and acceptor pharmacophore elements (*vide infra*) were constrained in the trans orientation. All chiral atoms were marked. Each search was continued until the global energy minima were found at least 3 times. The energy minimizations were carried out using the Polak-Ribiere-conjugate-gradient method[20] as implemented in MacroModel. Two force fields were used, OPLS-2005[21,22] and MMFFs.[23] Default parameters were used. The conformational searches were done for aqueous solution using the generalized Born/solvent accessible surface (GB/SA) continuum solvation model.[24,25]

Received: March 25, 2015
Published: May 29, 2015

DOI: 10.1021/acs.jcim.5b00159
J. Chem. Inf. Model. 2015, 55, 1435−1448

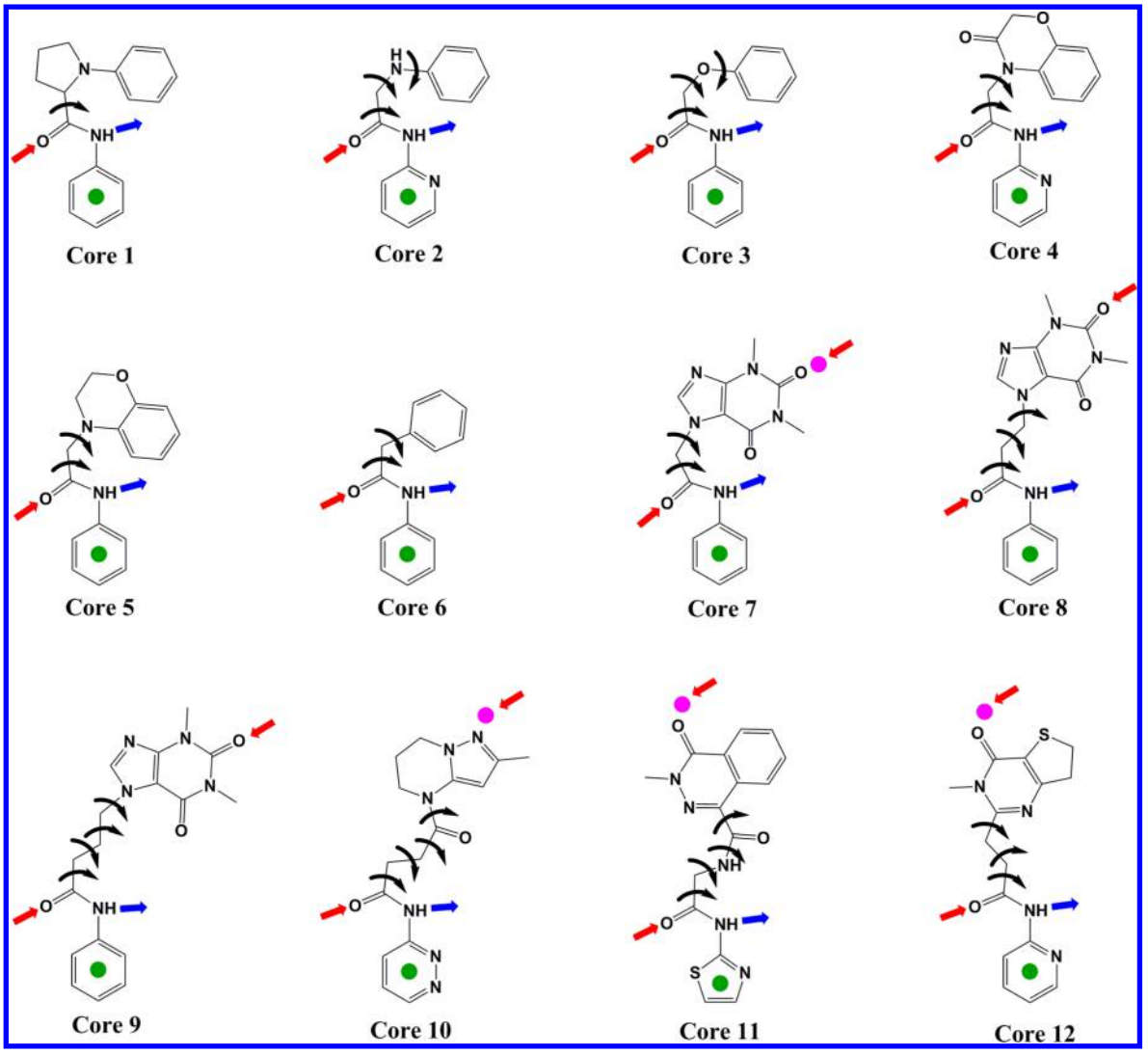

Figure 1. Definition of the cores of the scaffolds. In one experiment, the indicated torsions were constrained during the DFT minimization of the putative bioactive conformations. In another experiment, the putative bioactive conformations as well as the global energy minima found by OPLS2005 and MMFFs were minimized using DFT without constraints.

Table 1. Biological Activity, Conformational Energies and Fitting Parameters of Compounds Used for Construction of the Porcupine Pharmacophore Model[a]

		model A					model B				
		ConfE (kJ/mol)					ConfE (kJ/mol)				
compound	STF3a IC_{50} (μM)	OPLS205	MMFFs	DFT	RMSD (Å)	Φ (deg)	OPLS205	MMFFs	DFT	RMSD (Å)	Φ (deg)
1	0.036	9.3	19.2	0	0		0	7.8	1.1	0	
2	0.0009	10.2*	13.1	8.1	0.095		1.0*	3.6	0.5	0.26	
3	0.015	9.5	9.6	9.7	0.30		6.4	14.9	4.2	0.13	
4	0.002	17.6*	10.8	10.6	0.20		28.9*	29.9	23.9	0.10	
5	0.0003	7.3	16.3	1.8	0.25		0.8	3.8	2.1	0.32	
6	0.0005	4.2	2.7	0.2	0.28		0.8	7.5	1.4	0.20	
7	0.002	6.8	10.4	5.9	0.32	0	14.2	28.8	15.8	0.23	0
8	0.004	17.2	20.8**	8.6	0.32		26.1	32.2**	26.2	0.46	
9	0.004	26.9**	24.5**	6.3	0.24		40.2**	45.3**	22.0	0.28	
10	0.002	11.2	5.8	3.1	0.38	26.3	27.9	30.3	7.7	0.43	0
11	0.060	5.7	44.9**	3.2	0.91	33.2	6.8	39.1**	17.0	1.05	34.1
12	0.0005	4.0*	20.8**	0.6	0.14	27.9	6.4*	36.6**	3.6	0.17	22.5
average		10.8	16.6	4.8	0.29		13.3	23.3	10.5	0.30	

[a] *, error in forcefield; see the calculation of the conformational energy penalty under Computational Methods. **, electrostatic collapse in global energy minima.

DOI: 10.1021/acs.jcim.5b00159
J. Chem. Inf. Model. 2015, 55, 1435−1448

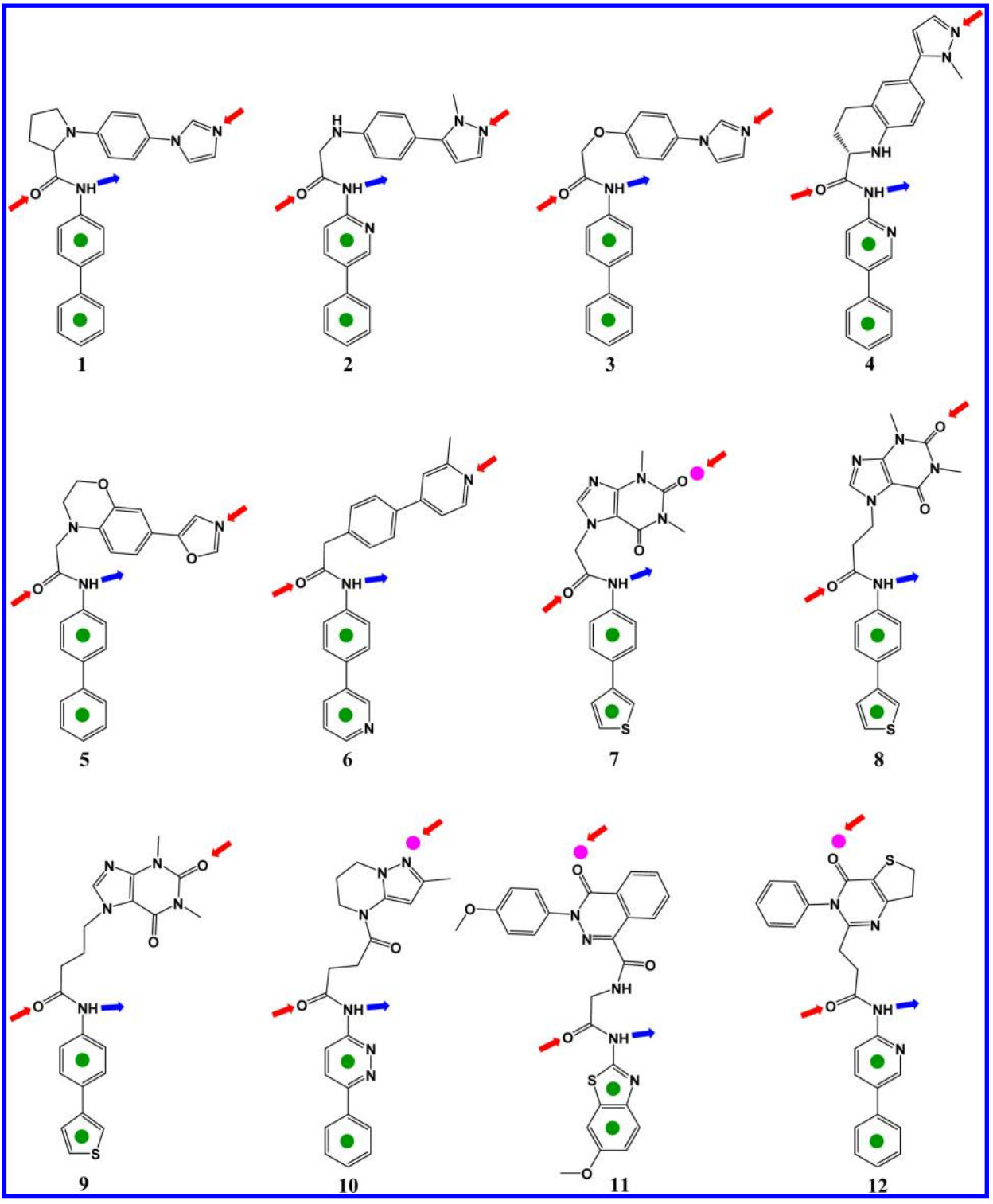

Figure 2. Structures of the structurally diverse set of potent porcupine inhibitors used for identifying the pharmacophore elements and construction of the porcupine pharmacophore model. The data for these compounds are shown in Table 1.

2.2. Calculation of the Conformational Energy Penalty. The conformations fitted to the pharmacophore models were minimized with MacroModel using flat bottom Cartesian constraint with a half width of 1.0 Å and a default restraining force constant of 100 kJ/mol. This allows the modeled conformations to relax and adjust to the force field.[21,22] Without the relaxation, the energy calculated by OPLS2005 and MMFFs may be grossly overestimated. This relaxation does not change the conformation as RMS values between the initial and relaxed structures are within 0.1 Å. The conformational energy penalty of the modeled conformations was calculated by subtracting the solution phase energy of the preferred conformation in aqueous solution (i.e., the energy of the global energy minimum in solution) from the calculated solution phase energy of the conformation fitted to the pharmacophore model. Since the conformational ensemble was represented by only the global energy minima,

DOI: 10.1021/acs.jcim.5b00159
J. Chem. Inf. Model. 2015, 55, 1435−1448

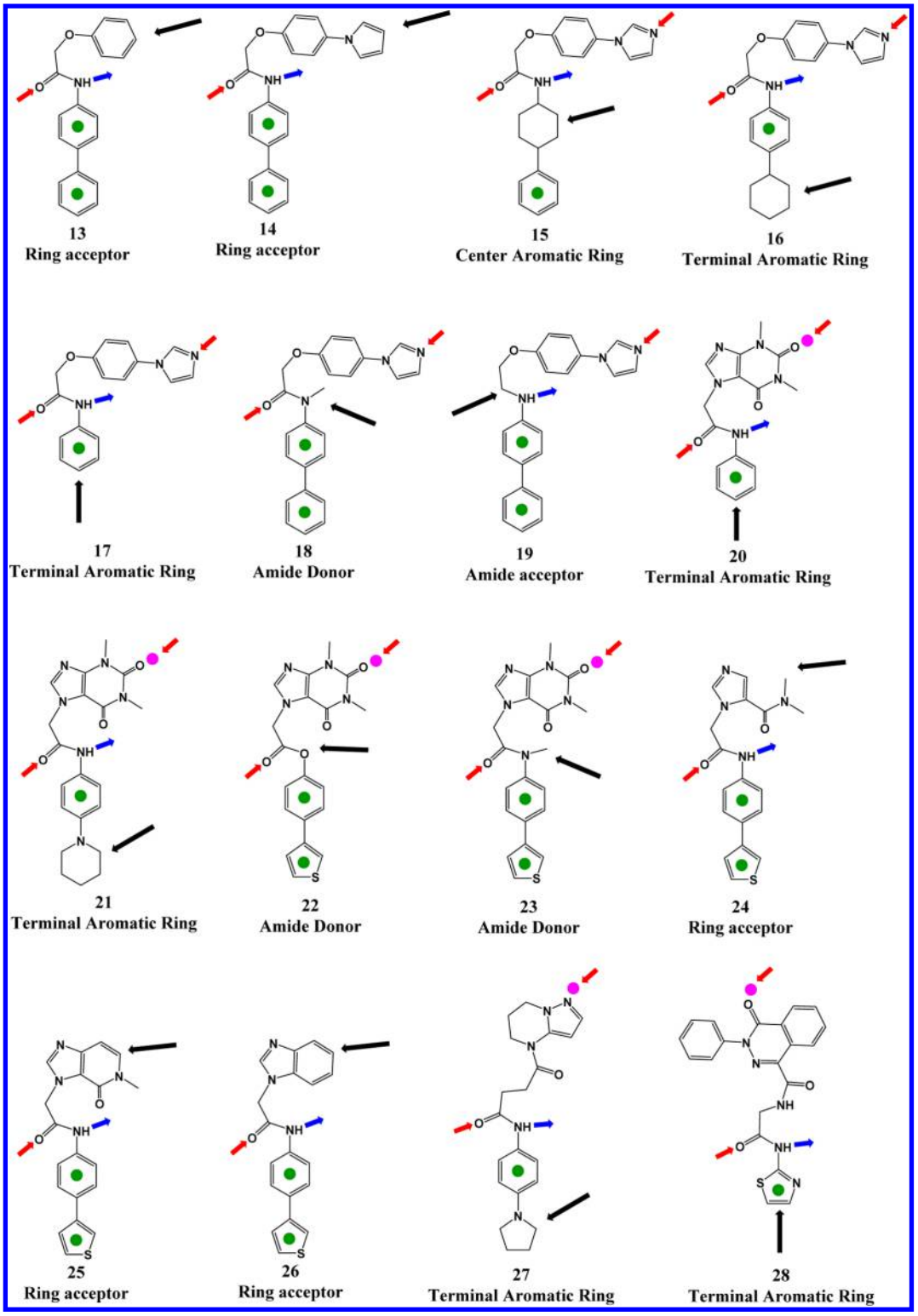

Figure 3. Inactive compounds missing a pharmacophore element as indicated by the black arrow. By comparing these compounds with their parent compounds (Figure 2 and Table 1) that are all potent inhibitors, the pharmacophore elements may be identified. The data for these compounds are shown in Table 2.

entropy effects have not been taken into account. For flexible molecules, this leads to an underestimation of the energy penalty. A limit of 3 kcal/mol (12.6 kJ/mol) for acceptable energy penalties was imposed as recommended by Boström et al.[26]

Compounds **2**, **4**, **12**, and **39** have a pyridine as the central aromatic ring next to the amide. In the lowest DFT energy conformation, the pyridine nitrogen is facing the amide donor. This conformation of the *N*-(pyridin-2-yl)acetamide fragment is 17.6 kJ/mol lower in energy than the conformation where the pyridine nitrogen is opposite the amide donor. However, in the OPLS-2005 force field this conformation is 7.9 kJ/mol higher in energy. Consequently, the OPLS-2005 global energy minima of

DOI: 10.1021/acs.jcim.5b00159
J. Chem. Inf. Model. 2015, 55, 1435−1448

Table 2. Biological Activity, Conformational Energies, and Fitting Parameters of Inactive or Less Active Compounds Lacking a Pharmacophore Element[a]

		model A			
		ConfE (kJ/mol)			
compound	STF3a IC_{50} (μM)	OPLS205	MMFFs	RMSD (Å)	Φ (deg)
13	>50	8.9	8.4	0.23	
14	>50	9.1	9.8	0.29	
15	>50	8.2	7.0	0.17	
16	>50	10.5	10.1	0.28	
17	>50	9.3	8.6	0.28	
18	2.2	12.8	12.2	0.33	
19	>50	7.0	15.0	0.23	
20	>50	6.4	9.0	0.31	0
21	0.53	8.0	9.0	0.33	0
22	>50	10.6	14.0	0.43	0
23	10.6	9.4	11.3	0.31	0
24	>50	10.2	11.0	0.19	
25	>50	9.2	7.5	0.24	
26	>50	1.6	2.7	0.19	
27	4.3	9.7	3.5	0.45	15.8
28	>25	3.5	37.8**	0.64	33.3

[a] **, electrostatic collapse in global energy minima.

these compounds were taken as the lowest energy conformation with the pyridine nitrogen facing the amide donor. Energies calculated like this are marked with an asterisk in the tables.

2.3. DFT Calculations. The program Jaguar, version 7.6[18] was used for B3LYP DFT energy minimization. The chosen basis set was 6-31G**. The PBF solvation model[27] was used with water as solvent. Accuracy level was set to "Accurate," and grid density was set to "Fine". DFT calculations were done on fragments rather than whole molecules. These fragments consisted of the scaffold core as indicated in Figure 1. A DFT minimization was done for the cores fitted to each of the pharmacophore models (with constrained torsions as indicated in Figure 1) and on each of the global energy minima found by OPLS2005 and MMFFs without using constraints. The resulting conformation with the lowest energy was taken as the global DFT energy minima.

2.4. Superimposition Procedure. Two aromatic rings, one amide acting both as hydrogen bond donor and acceptor and an additional acceptor referred to as ring acceptor (a ring system carbonyl oxygen or aromatic nitrogen) were chosen as pharmacophore elements. For each of the aromatic ring pharmacophore elements, centroids were constructed. The compounds were first superimposed on the pharmacophore model using these centroids and the amide donor and acceptor atoms as fitting points. If the ring acceptor atom approximately overlaid with the one of the pharmacophore model, this was included as a fitting point. If not, it was assumed that this hydrogen bonding interaction was mediated by a water molecule and the following procedure was used.

(1) In order allow for some flexibility in the directions of the hydrogen bond, a dummy atom was placed in the plane of the ring 2.8 Å from the donor/acceptor atoms in the direction of the putative hydrogen bond interaction vector defined by the pharmacophore model. Thus, the ideal hydrogen bond geometry (where the acceptor lone pair and donor hydrogen lie on a straight line between the heavy atoms) was not necessarily employed.

(2) The compounds were then again fitted to the pharmacophore models now using both the centroids and the dummy atoms described above as fitting points. The RMS values in Table 1 were obtained from this second fit. The ring hydrogen bond acceptor atom in the molecules was not used in the superimposition if the dummy atom was used.

(3) In order to evaluate the angle of deviation from an ideal hydrogen bond direction, a second hydrogen bonding site point was represented by a dummy atom 2.8 Å from the donor/acceptor atom in the direction of the lone pair for nitrogen acceptors or along the axis of the carbon−oxygen bond for carbonyl acceptors.

(4) The angle of deviation between the actual hydrogen bonding direction and the ideal direction was then calculated. This angle, ϕ, is given in Table 1 for molecules where the dummy atom was used as a fitting point.

Least-squares rigid body molecular superimpositions were performed using Maestro. The superimpositions were evaluated in terms of RMS values of the fitting points. An RMS value of 0.5 Å has been used as a soft indicator to determine whether a fit is acceptable or not. The aromatic pharmacophore elements were fitted in a coplanar orientation if energetically possible. The RMS values do not give any measure of this coplanarity since only the centroids are superimposed.

2.5. Calculation of Physical Properties. The program QikProp 4.2[18] was used to calculate logP and polar surface area (PSA). Rotatable bonds were counted manually excluding aliphatic ring bonds and amide bonds.

2.6. Synthetic and Analytical Chemistry. All compounds except **6**, **11**−**12**, and **28** were conceived and synthesized by the medicinal chemistry group of the Experimental Therapeutics Centre (ETC). These compounds are previously unpublished. The synthesis of compounds **1**−**5** and **33**−**41** as well as analytical validation by LC/MS and NMR is described in the patent applications GB1307564.3.[28] Synthesis of compounds **7**−**9** and **42**−**44** is described in the patent applications GB1309333.1.[29] Synthesis of compounds **10**, **46**, and **47** is described in the patent applications GB1322333.4,[30] GB1409783.6,[31] and GB1322334.2,[32] respectively. The synthesis of the reference compound **6** was done in ETC and described in the Novartis patent application PCT/US2011/042215.[33] Compounds **11**−**12** and **28** have been published by The University of Texas Southwestern Medical Center.[34] Synthesis and characterization of compound **45** is described in the Supporting Information.

2.7. Cell-Based Assays. All assay data except for compounds **11**−**12** were generated by the cell-based assay development group of the Experimental Therapeutics Centre. Data for compound **11**−**12** were taken from the literature.[34]

TOPFlash Assays. The assay used to determine the IC_{50} of the compounds was done as described in Coombs et al.[12] but with the following modifications: 2×10^4 STF3A cells were seeded in each well of a 96 well plate (Greiner) and incubated overnight at 37 °C. 25 μL of serially diluted compound was added to the cells to give final concentrations of 50 μM to 1.5 nM. After 1 day of treatment, 100 μL of Steady-Glo Luciferase Assay reagent (Promega) was added to each well and incubated for 10 min at room temperature. Luminescence was measured using a Tecan Safire2 plate reader.

To confirm that the compounds inhibited Wnt secretion, HEK293-STF cells with no Wnt3A expression was used. L-Wnt3A cells were cultured in three T-175 flasks at 3×10^4 cells/mL in a 30 mL culture medium per flask. After 4 days of incubation,

DOI: 10.1021/acs.jcim.5b00159
J. Chem. Inf. Model. 2015, 55, 1435−1448

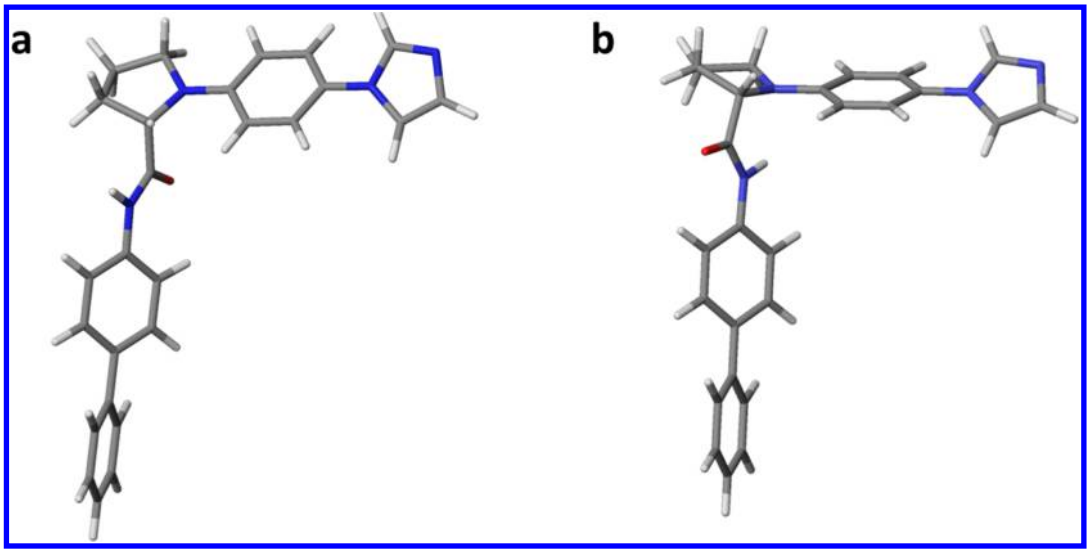

Figure 4. Two classes of conformational energy minima of the proline scaffold (compound **1**). Conformation A (left) is higher in energy than conformation B (right) calculated by OPLS2005 and MMFFs, but the DFT energy is the same for the two shown conformations.

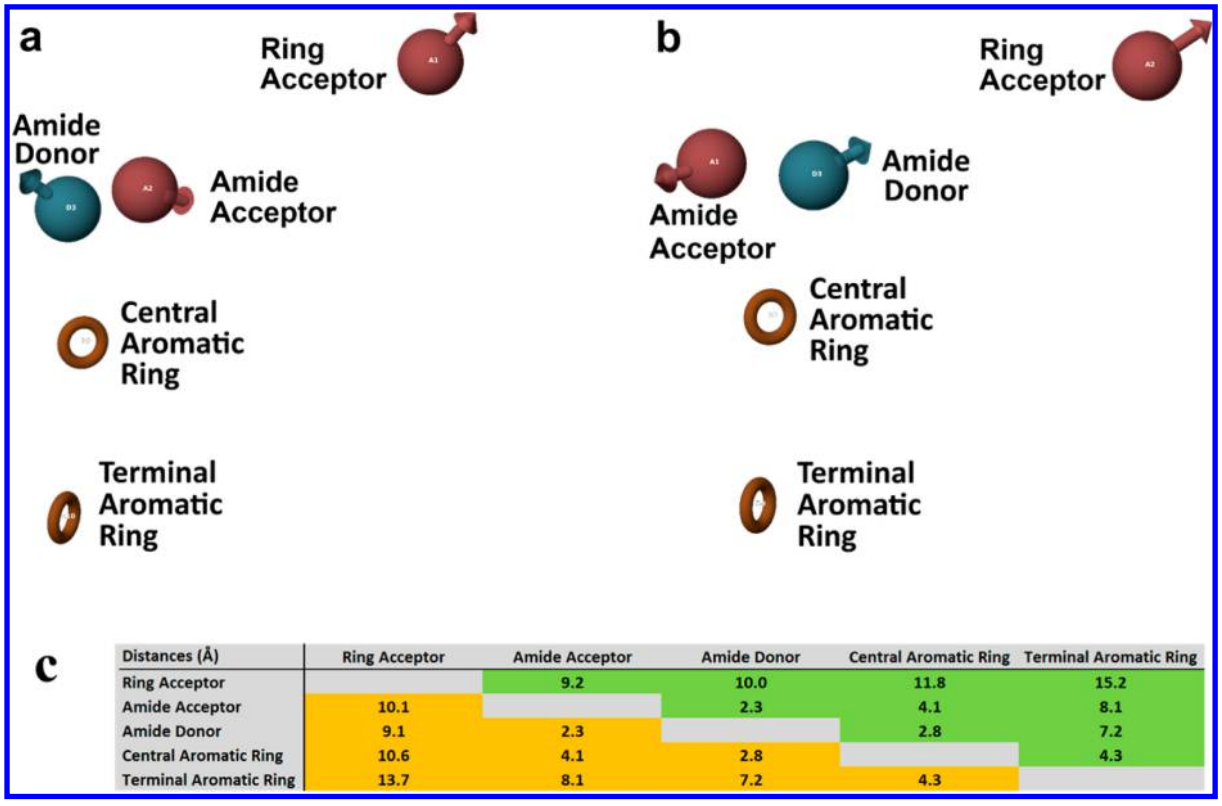

c

Distances (Å)	Ring Acceptor	Amide Acceptor	Amide Donor	Central Aromatic Ring	Terminal Aromatic Ring
Ring Acceptor		9.2	10.0	11.8	15.2
Amide Acceptor	10.1		2.3	4.1	8.1
Amide Donor	9.1	2.3		2.8	7.2
Central Aromatic Ring	10.6	4.1	2.8		4.3
Terminal Aromatic Ring	13.7	8.1	7.2	4.3	

Figure 5. Two possible pharmacophore models based on the minima of the proline scaffold. (a) Pharmacophore model A is the most probable due to the lower conformational energies of compounds fitted to this model (see Table 1). (b) Pharmacophore model B. (c) Distances between the centroids and heavy donor/acceptor atoms that define pharmacophore model 1 (green cells) and pharmacophore model 2 (orange cells).

the Wnt3A conditioned media were harvested. HEK293-STF cells (2×10^4) in 25 μL culture media were added to each well of a 96 well plate (Greiner). Twenty-five microliters of serially diluted compound was added. After 4 h of incubation, 100 μL of Wnt-3A conditioned medium was added to the cells. The final concentration of compound ranged from 33 μM to 1 nM. After incubation for 1 day at 37 °C, 100 μL of Steady-Glo Luciferase Assay reagent (Promega) was added to each well and incubated for 10 min at room temperature. Luminescence was measured using a Tecan Safire2 microplate reader.

3. RESULTS AND DISCUSSION

3.1. Compound Selection and Pharmacophore Elements.

The potent porcupine inhibitors **1**−**12** (Figure 2 and Table 1) were used to derive the pharmacophore model. These have 4−7 rotatable bonds excluding amide bonds. The logP was calculated

DOI: 10.1021/acs.jcim.5b00159
J. Chem. Inf. Model. 2015, 55, 1435−1448

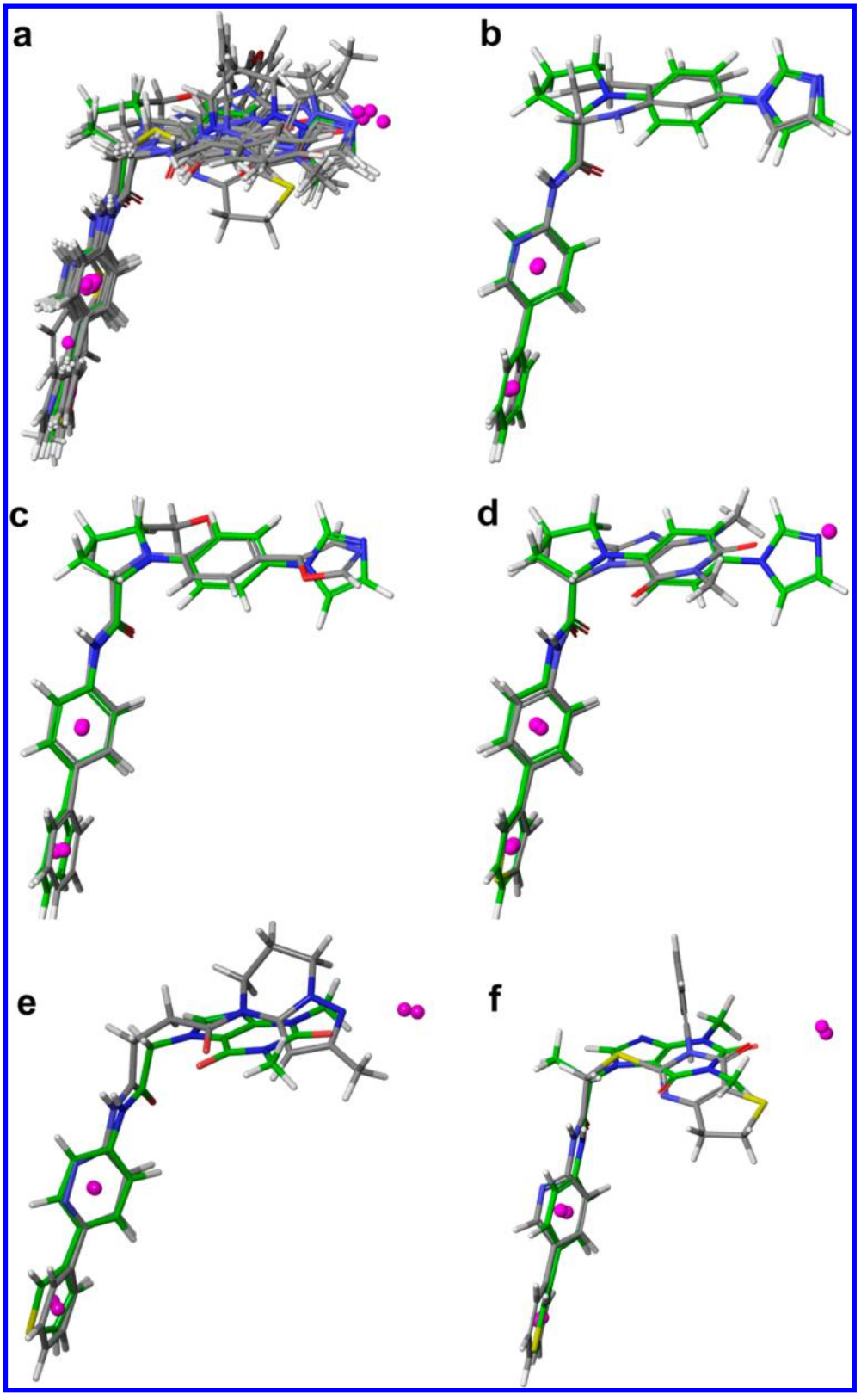

Figure 6. Superimposition of compounds from Table 1 on pharmacophore model A. Centroids and ring acceptor sidepoints are shown as magenta balls. (a) Superimposition of all compounds. Compound **1** is shown with green carbon. (b) Superimposition of compounds **1** and **4**. Compound **1** is shown with green carbon. (c) Superimposition of compounds **1** and **5**. Compound **1** is shown with green carbon. (d) Superimposition of compounds **1** and **7**. Compound **1** is shown with green carbon. (e) Superimposition of compounds **7** and **10**. Compound **7** is shown with green carbon. (f) Superimposition of compounds **7** and **12**. Compound **7** is shown with green carbon.

to be high, varying between 3.2 for xantine compound **7** to 5.8 for proline **1**, and one of the main challenges of the project was to increase solubility. The polar surface area (PSA) was calculated to be below 110 Å^2 except for compound **11** (PSA of 140), and

DOI: 10.1021/acs.jcim.5b00159
J. Chem. Inf. Model. 2015, 55, 1435−1448

Table 3. Biological Activity, Conformational Energies, and Fitting Parameters of Enantiomeric Pairs Used for Evaluating the Model[a]

		model A				
		ConfE (kJ/mol)				
compound	STF3a IC_{50} (μM)	OPLS205	MMFFs	DFT	RMSD (Å)	Φ (deg)
1S	0.036	9.3	19.2	0	0	
1R	33	18.4	43.3	22.2	0.67	
29S	0.001	9.9**[c]	9.6	2.5	0.089	
29R	0.64	20.8**	28.3	20.7	0.11	
30S	0.007	8.7	4.5	6.2	0.31	
30R	0.13	28.3	29.58	31.6	0.32	
4S	0.002	16.1**	10.8	10.6	0.20	
4R	0.023	12.6**	21.0	15.6	0.29	
31S	0.0004	8.4	8.8	6.4	0.37	0
31R	>50	24.5	17.8	15.9	0.30	0
32R	0.002	14.4	6.0	1.6	0.39	26.2
32S	13.7	25.9	18.5	13.1	0.35	26.2
average *S*[b]		11.1	9.8	4.6	0.23	
average *R*[b]		21.8	26.4	19.9	0.34	

[a]These compounds are shown in Figure 7. Average *S* is the average conformational energy of the more active (*S*)-enantiomers, and average *R* is that of the less active (*R*)-enantiomers. [b]**32R** was included in average *S*, and **32S** was included in average *R* as the stereochemistry for this pair is opposite that of the other enantiomeric pairs. [c] **, error in forcefield; see the calculation of the conformational energy penalty under Computational Methods.

cell permeability was not found to be a problem. Compounds **1**−**5** and **7**−**10** were synthesized in our laboratory during the optimization of various HTS hits. Among these compounds, **1**, **4**, and **5** are conformationally restricted analogues which were important for the determination of the bioactive conformation. Compound **6** is C59, an early derivative of the eventual Novartis development compound LGK974.[33] Compounds **10** and **11** were reported by the group from the University of Texas.[34] A superficial examination of the 12 structures in Figure 2 suggests that **1**−**5** are probably closely related, while the linker and the northern part are quite distinct for structures **7**−**12**.

To identify the pharmacophore elements, we looked for analogues of highly potent compounds that only differed by lacking a specific atom or group. The compounds in Figure 3 and Table 2 are derivatives of **1**−**12** that are inactive or much less potent porcupine inhibitors but still able to adopt the same putative bioactive conformation as the more active analogues. These compounds are therefore inactive or less active due to lacking pharmacophore elements and not because of conformational issues. We identified the pharmacophore elements as the groups or atoms present in **1**−**12** but lacking in those from Figure 3.

Compounds **1**−**6** have an aromatic nitrogen donor in the form of an imidazole, oxazole, pyrazole, or pyridine ring. This is lacking in **13** and **14** rendering the compounds inactive. The xanthines **7**−**9** have a carbonyl donor that is essential for activity, as the compounds **24**−**26** lacking this acceptor are inactive. Thus, all potent porcupine inhibitors have an acceptor in this area. We will refer to this pharmacophore element as the ring acceptor. In **15**, the central aromatic ring has been replaced by a cyclohexyl rendering the compound inactive. In compounds **16**−**17**, **20**−**21**, and **27**−**28**, the terminal aromatic ring has been removed or replaced by an aliphatic group rendering the compounds inactive or 200−1000-fold less active for **21** and **27**. Thus, both the aromatic rings are essential for high activity. In **22**, the amide is replaced by an ester, and in **18** and **23**, the amide nitrogen is methylated. The ester **22** is inactive, and the free amides **3** and **7** are 100−5000-fold more potent than the methylated analogues indicating that the amide donor is essential for potent inhibition. In compound **19**, the amide carbonyl has been replaced by a methylene that renders the compound inactive. Thus, 5 pharmacophore elements were identified: the amide donor and acceptor, the two aromatic rings, and an additional ring acceptor atom that may be an aromatic nitrogen or a carbonyl oxygen. The pharmacophore elements are shown with centroids and arrows in Figure 2.

3.2. Construction of the Pharmacophore Model. The most constrained compound is the proline **1**. Ignoring the phenyl and imidazole rotamers, compound **1** only has 2 low energy conformations. Conformation A has the amide carbonyl pointing below the plane of the phenyl-pyrrolidine-imidazole. Conformation B has the amide donor pointing below the plane of the phenyl-pyrrolidine-imidazole (Figure 4). Conformation A is 9.3 and 14.8 kJ/mol higher in conformational energy than conformation B calculated by OPLS-2005 and MMFFs, respectively. However, the DFT energy difference of the two conformations is low at 1.1 kJ/mol. A pharmacophore model was developed for each of these conformations using the proline compound **1** as a template. The phenyl and imidazole rotamers were chosen as shown in Figure 4. All compounds used to derive the models have aromatic rings analogous to the two phenyls in **1**. These were fitted in a coplanar orientation. The torsion of these rings may be important if they are substituted, but our SAR indicated that only minor substituents were allowed (data not shown). The torsion is also important when the central aromatic ring is a pyridine as in **2**, **4**, and **12**. In this case, the pyridine nitrogen was modeled to face the amide donor as this is the lowest energy conformation. All compounds were fitted with the amide donor and acceptor pointing in the same direction as those in the template. For compounds **1**−**6** and **8**−**9**, the ring acceptor pharmacophore element overlaid well. However, this is not the case with **7** and **10**−**12**. For these compounds, it was observed that the ring acceptor was approximately 2.8 Å from that of the template. Thus, it was hypothesized that in these compounds, the ring acceptor hydrogen bonds to the porcupine protein through a water molecule. Consequently, a dummy atom was constructed 2.8 Å from the ring acceptor in the direction of the lonepair, and this was used as a fitting point for these compounds (see Computational Methods).

The conformational energy of the modeled conformations was calculated by subtracting that of the global energy minima. This was done for conformations fitted to both models using OPLS-2005, MMFFs, and DFT (see Computational Methods). The energies are given in Table 1 together with the RMSD of the fitting points. There is little difference in the average OPLS-2005 energy between the two models (<3 kJ/mol). The conformational energy is on the high side for 3 and 4 of the compounds when fitted to model A and B, respectively. The conformational energies calculated by MMFFs was somewhat higher than the OPLS-2005 energies, but there was a clear difference between the two models with the average conformational energy being 6.7 kJ/mol lower for model A. The MMFFs global energy minima of compounds **8**−**9** and **11**−**12** were collapsed with the aromatic rings adopting nonlinear conformations with intramolecular stacking interactions. These may not be true global

DOI: 10.1021/acs.jcim.5b00159
J. Chem. Inf. Model. 2015, 55, 1435−1448

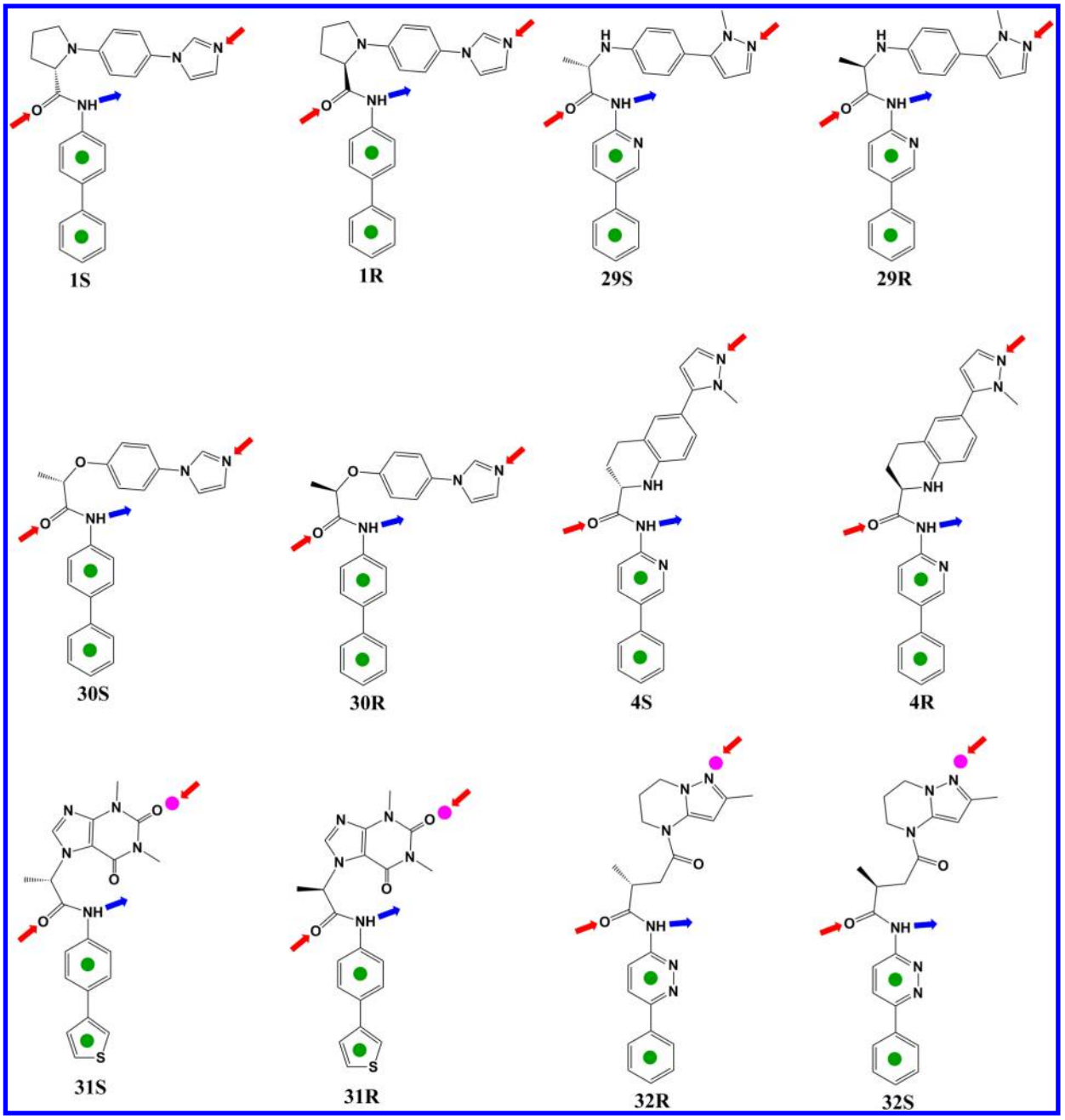

Figure 7. Chiral compounds used for validating the pharmacophore model. The data for these enantiomeric pairs are shown in Table 3.

energy minima resulting in an overestimation of the conformational energy. Electrostatically collapsed conformations were generally not found using the newer OPLS-2005 force field. The average DFT energy was low for both models with model A being 5.7 kJ/mol lower than that of model B. All conformations fitted to model A had low DFT energies, while 5 conformations fitted to model B were slightly higher in energy. The two pharmacophore models are shown in Figure 5. The average RMSD of conformations fitted to models A and B was similar at 0.29 and 0.30 Å, respectively. The DFT and MMFFs conformational energy calculations clearly point to model A being the best pharmacophore model; consequently, this was chosen to represent the bioactive conformations.

After the models were derived, the inactive compounds used for identifying the pharmacophore elements (Figure 3) were fitted to model A. For all of these compounds, a conformation similar to that of the putative bioactive conformation of the parent compound (i.e., compounds **3**, **7**, **10**, and **11**) was identified. These conformations fitted to the model with low RMSD and low conformational energies (Table 2) showing that the significantly reduced activity of these compounds may be due to the lack of pharmacophore elements.

Figure 6a shows a superimposition of all compounds used for deriving the pharmacophore model. The two aromatic ring pharmacophore elements are coplanar in all of these compounds. The phenyl-imidazole, xanthine, and other ring systems holding the ring-acceptor pharmacophore element are also roughly coplanar. In Figure 6b and c, compounds **4** and **5**, respectively are superimposed on **1**. The pyrazole and oxazole of **4** and **5** superimpose very well on the imidazole of **1** with the nitrogen acceptors within 0.1 Å. Figure 6d–f shows compounds **1**, **10**, and **12** superimposed on the xanthine compound **7**. The dummy

DOI: 10.1021/acs.jcim.5b00159
J. Chem. Inf. Model. 2015, 55, 1435−1448

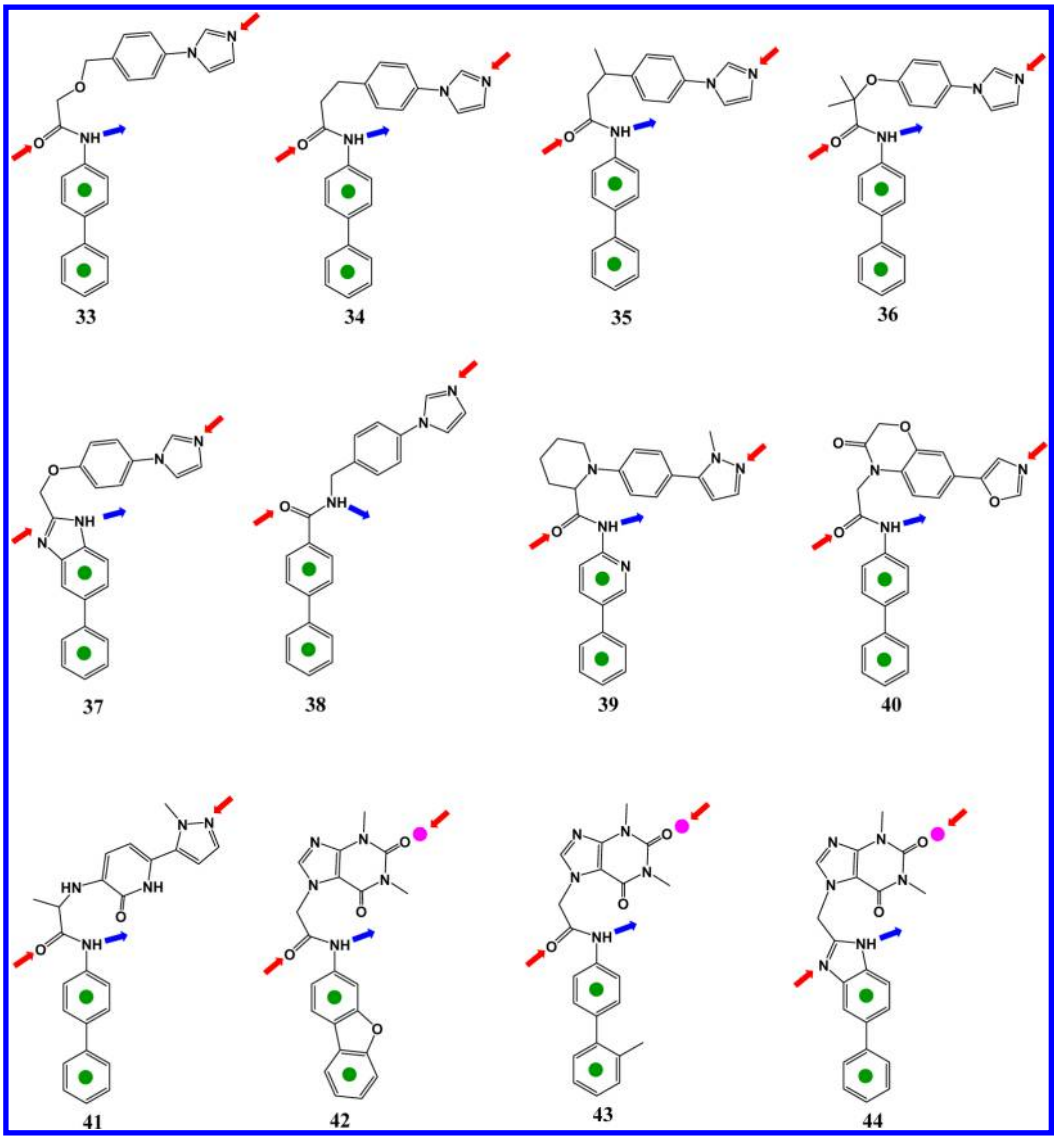

Figure 8. Compounds with scaffold modifications used for validating the pharmacophore model. The data for these compounds are shown in Table 4.

atom 2.8 Å from the xanthine carbonyl is within 0.3 Å of the imidazole acceptor of **1** as shown in Figure 6d. For **10**, the dummy atom and ring acceptor superimpose well on that of the xanthine **7**, while the carbonyl directly attached to the dihydropyrazolo-pyrimidine superimposes with the other xanthine carbonyl (Figure 6e). In the superimposition of **12** on **7**, both the dummy atom and ring acceptor superimpose well, while the nitrogen acceptor of the tetrahydrothieno-pyrimidinone ring system superimposes on the other xanthine carbonyl (Figure 6f).

3.3. Evaluation of the Pharmacophore model. 1: Enantioselectivity. Compounds **1** and **4** are chiral, and for both of these, the S-enantiomer was used for constructing the pharmacophore model. For **1**, the S-enantiomer is 1000-fold more potent than the R-enantiomer, while for compound **4** this difference is only 10-fold (Table 3). During our porcupine project, several other chiral compounds were synthesized as shown in Figure 7. These compounds may be used for evaluating the pharmacophore model. The most active enantiomer should be the one that fits best to the model. If both enantiomers fit well, the conformational energy of the less active enantiomer may be higher, or the compound may clash with the receptor. Of all the enantiomeric pairs, both enantiomers may be fitted to the pharmacophore model with low RMSD (Table 3). However, when the less active enantiomers were fitted to the model the coplanarity of the phenyl-imidazole, phenyl-pyrazole, and xanthine rings was not taken into account. These were approximately 90° to those of the more active enantiomer.

The average conformational energy of the more active enantiomer was substantially lower than that of the less active enantiomer as calculated by OPLS-2005, MMFFs, and DFT. The average energy difference was approximately 10 kJ/mol in OPLS-2005 and 15 kJ/mol for MMFFs and DFT. For MMFFs and DFT, all the more active enantiomers were lower in energy than the less active ones, while for OPLS-2005 this was the case for 5 of the 6 enantiomeric pairs. The OPLS-2005 energy of **4S** was slightly higher than that of the less active **4R**. However, this enantiomeric pair is the one with the least difference in porcupine inhibitory activity. On the basis of conformational energies, the model was able to distinguish between the enantiomeric pairs.

3.4. Evaluation of the Pharmacophore Model. 2: Scaffold Modifications. Compounds **33**–**36** (Figure 8) are analogues of the ether linked **3** with linker modifications. Compound **33** has an extra methylene inserted between the

DOI: 10.1021/acs.jcim.5b00159
J. Chem. Inf. Model. 2015, 55, 1435−1448

Table 4. Biological Activity, Conformational Energies, and Fitting Parameters of Compounds with Scaffold Modifications Used for Evaluating the Model (Figure 8)[a]

		model A				
		ConfE (kJ/mol)				
compound	STF3a IC_{50} (μM)	OPLS205	MMFFs	DFT	RMSD (Å)	Φ (deg)
33	11.6	15.9	20.2	14.1	0.48	
34	0.092	17.7	14.8	7.5	0.045	
35 (S)	>50	31.1	27.0	13.3	0.06	
35 (R)	>50	20.9	17.5	2.6	0.06	
36	>50	17.0	13.1	12.5	0.095	
37	3.1	10.7	20.2	7.6	0.71	
38	>50	2.1	8.4	4.7	0.44	
39	2.1	15.7*	18.1	6.7	0.14	
40	0.005	1.0	2.7	1.3	0.14	
41 conf1	0.021	40.5	20.6	23.8	0.21	
41 conf2	0.021	18.7	13.9	2.1	0.30	
42	0.016	6.8	8.2	3.2	0.35	0
43	0.048	9.9	12.0	4.6	0.27	0
44	5.0	5.8	8.9	0	0.73	0
45	0.005	7.3	11.0	5.5	0.17	0
46	0.002	6.8	8.5	0.2	0.28	14.0
47	0.015	4.8	10.5	0.1	0.27	21.8

[a]Compounds **45** (S enantiomer) and **46**–**47** are examples of novel scaffolds designed using the pharmacophore model (Figures 9–10). *, error in force field; see the calculation of the conformational energy penalty under Computational Methods

oxygen and aromatic ring compared to **3**. As a result of the one atom longer linker, **33** could only be fitted to the model with a somewhat high conformational energy and RMSD (Table 4). This is in line with the much reduced activity of **33** compared to that of **3**. Compound **34** is an analogue of **3** with the ether oxygen replaced by a methylene. Although the methylene is not conjugated with the phenyl like the ether oxygen of **3**, this is both structurally and electrostatically a small change, and **34** could be fitted with low conformational energy and low RMSD consistent with the slight loss of activity compared to that of **3**. Compound **35** is a methyl analogue of **34**. The RMSD and conformational energy of the putative bioactive conformation of the R-enantiomer is similar to that of **34**, but the S-enantiomer is high in conformational energy. This is opposite the enantiomeric pairs in Figure 7, where the S-enantiomer has the lowest energy bioactive conformation. Compound **35** is devoid of measurable activity probably due to the high energy of the S-enantiomer and the R-enantiomer clashing with the protein. Compound **36** is the dimethyl analogue of **30S** and **30R**. Although the RMSD is low and conformational energy of the putative bioactive conformation of **36** is not too high, the compound lost all activity. This is probably also due to a steric clash between the protein and methyl that superimpose with the methyl of compound **30R**.

Compounds **37**–**38** are analogues of **3** with amide modifications. Compound **37** is a benzimidazole analogue. Benzimidazole is a common bioisostere for phenylamide, but **37** had much reduced activity. Although the conformational energy was low, **37** could not be fitted to the model with low RMSD. In **38**, the amide has been reversed as compared to **34** but with complete loss of activity. A low energy conformation of **38** could be fitted to the model with a moderately high RMSD. As the amide oxygen and amide hydrogen were used as fitting points, the RMSD was not that high, but if the interaction points (i.e., dummy atoms 2.8 Å from the oxygen and hydrogen in the direction of an ideal hydrogen bond) had been used, the RMSD would have been much higher.

Compounds **39**–**41** are analogues of the N-linked compounds **1**, **2**, and **5**. Compound **39** is a piperidine analogue of proline **1**. Compound **39** was fitted to the model with low RMSD and low conformational energy as calculated by DFT, although the conformational energy calculated by the molecular mechanics was high. The reduced activity of **39** is probably due to the increased bulk of the piperidine ring clashing with the protein. Compound **40** is an amide analogue of the fused morpholine compound **5**. Compound **40** could be fitted to the pharmacophore model with low conformational energy and low RMSD. The addition, the carbonyl relative to **5** did not change the conformation of the fused morpholine and linker. Although **40** remains highly active, it is 10-fold less active than **5**. The decreased affinity may be due to a change in cell permeability. Compound **41** is a pyridone analogue of **2** and was conceived as a hybrid between **2** and **7**. Pyridone may be fitted in two orientations, either with the carbonyl forming an intramolecular hydrogen bond to the linker NH which is a low energy conformation or with the carbonyl opposite the linker NH which is a high energy conformation. In the latter conformation, the pyridone carbonyl superimposes on one of the xanthine carbonyls of **7**. This is the xanthine carbonyl that is not a pharmacophore element. Although it is aesthetically appealing to fit the pyridone so the carbonyl superimposes with the xanthine carbonyl, the conformational energy points to the other conformation as being the bioactive conformation of **41**.

Compounds **42**–**44** are analogues to xanthine **7**. In **42**, the biphenyl has been locked into a coplanar orientation by a dibenzofurane as the torsional angle of the biphenyl has been increased in **43** by the addition of a methyl in the ortho position of the terminal phenyl. The conformational energy and RMSD of the putative bioactive conformation of both **42** and **43** were low. Variation in the torsion between the aromatic rings is clearly tolerated to some extent as the activity of **42**–**43** remains, although it is approximately 10–20-fold reduced compared to that of **7**. Like **37**, **44** is a benzimidazole analogue with much reduced activity. Compound **44** could only be fitted to the model with a high RMSD, but the conformational energy of this conformation was low.

3.5. Using the Pharmacophore Model for the Design of New Scaffolds. It was noted in the superimposition of the xanthine compound **7** and the proline compound **1** (Figure 6d), that the proline ring occupies an area corresponding to the methyl substituent in the linker of **7S** and a substituent in the xanthine 8-position. Consequently, it was proposed to cyclize these two positions to form the easily synthetically accessible tricyclic xanthine compound **45**, which is a hybrid of the xanthine and proline scaffolds (Figure 9). The putative bioactive conformation of **45** has low conformational energy and low RMS. Although **45** was found to be approximately equipotent with **7**, the tricyclic xanthines were generally slightly less potent. As predicted, the (S)-enantiomer of **45** was found to be the more active enantiomer, while the (R)-enantiomer did not have any measurable activity.

The phthalimide group of **46** superimposes well on the xanthine of **7** with the two carbonyls and the central N-Me being overlaid. In Figure 10, **46** is superimposed on **1**. The aromatic ring and amide pharmacophore elements superimpose perfectly, while the dummy atom of the ring acceptor of **46** is within 0.1 Å of the ring acceptor of **1**. This proposed bioactive conformation

DOI: 10.1021/acs.jcim.5b00159
J. Chem. Inf. Model. 2015, 55, 1435–1448

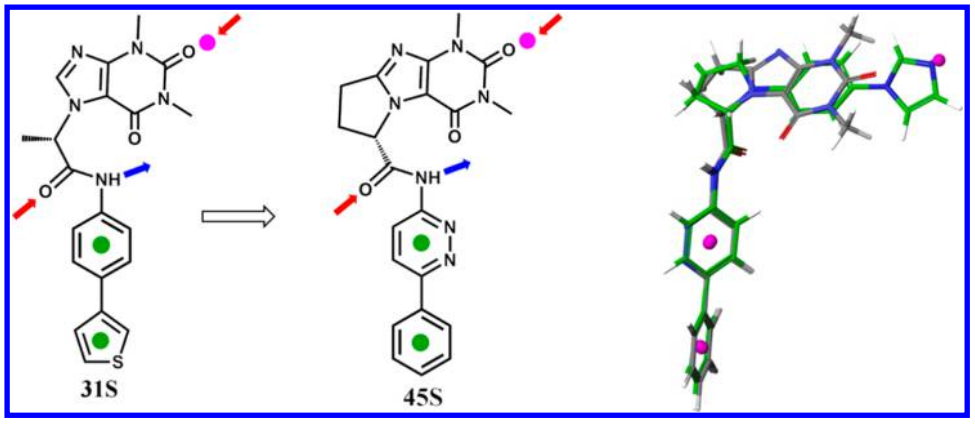

Figure 9. Tricyclic scaffold obtained by ligand-based design (left). The tricyclic scaffold (compound **45**, gray carbon) superimposed on the proline scaffold (compound **1**, green carbon). Centroids and the ring acceptor sidepoint are displayed as magenta balls. Notice how the proline rings of the two scaffolds are overlaid. The data for **45** are shown in Table 4.

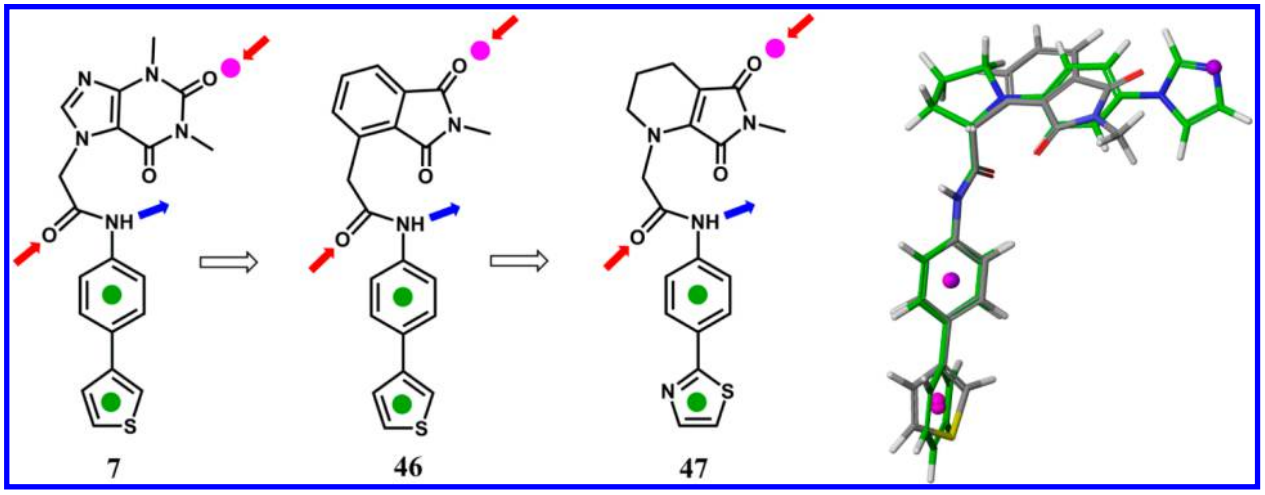

Figure 10. Phtalimide and maleimide scaffolds obtained by ligand-based design (left). The phtalimide scaffold (compound **46**, gray carbon) superimposed on the proline scaffold (compound **1**, green carbon). Centroids and the ring acceptor sidepoint are displayed as magenta balls. The data for **46**–**47** are shown in Table 4.

has a low conformational energy calculated both by DFT and both the force field methods. Consequently, the phthalimide in **46** was proposed to be a suitable bioisostere for the xanthine. When synthesized, the phatalimide series proved to be more potent than the xanthines. The phtalimide scaffold was further modified to the unsaturated fused piperidine–maleimide scaffold of **47**. Conformationally, this compound is very similar to the phthalimide **46** although slightly less potent.

4. CONCLUSIONS

Porcupine is a promising oncology target in the Wnt pathway. We have derived a pharmacophore model for porcupine inhibitors based on several scaffolds discovered in-house and 3 published scaffolds. The model consists of 5 pharmacophore elements: two aromatic rings, an amide donor, and acceptor as well as an additional acceptor atom. All currently published porcupine inhibitors may be fitted to the model in low energy conformations with good overlap of the pharmacophore elements. The model was evaluated by fitting the enantiomeric pairs of 6 different scaffolds to the model as well as other compounds with scaffold modifications. In all cases, the putative bioactive conformation of the more active enantiomers were found to be lower in energy than those of the less active enantiomer. Finally, we showed how the pharmacophore model may be used for ligand based drug design. On the basis of the putative bioactive conformation of the xanthine compound **7**, we designed 3 series of highly potent porcupine inhibitors with novel scaffolds.

■ ASSOCIATED CONTENT

Ⓢ Supporting Information

Structures of compounds **1**–**47** and dummy atoms fitted to pharmacophore model 1; structures of compounds **1**–**12** and dummy atoms fitted to pharmacophore model 2; activity data; outline of the synthesis and characterization of compound **45**; and a description of the Wnt palmitoylation assay. The Supporting Information is available free of charge on the ACS Publications website at DOI: 10.1021/acs.jcim.5b00159.

■ AUTHOR INFORMATION

Corresponding Author

*Tel: +65 6478 8767. Fax: +65 6478 8768. E-mail: apoulsen@etc.a-star.edu.sg.

Author Contributions

The manuscript was written by A.P. except for the Introduction and description of assays which were written by M.A.L. All

DOI: 10.1021/acs.jcim.5b00159
J. Chem. Inf. Model. 2015, 55, 1435–1448

molecular modeling was done by A.P. The compounds were conceived of and/or synthesized by S.Y.H., W.W., J.A., D.A.J., A.S.H., E.S.W.T., G.R.L., V.W.W.C., A.P., and T.K. Biological assays were done by Z.K. and M.A.L.

Notes

The authors declare the following competing financial interest(s): All authors are current or former employees of the Experimental Therapeutics Centre. This institute has a commercial interest in the development of WNT secretion inhibitors.

■ ACKNOWLEDGMENTS

We thank Shermaine Q. Y. Lim and Sifang Wang, ETC, for running the TOPFlash Assay. STF3A cells were kindly provided by David Virshup, Duke-NUS, Singapore.

■ ABBREVIATIONS

Wnt, Wingless-type; DFT, density functional theory; RMSD, root mean square deviation; MMFF, Merck molecular force field; OPLS, optimized potentials for liquid simulations force field

■ REFERENCES

(1) Klaus, A.; Birchmeier, W. Wnt Signalling and its Impact on Development and Cancer. *Nat. Rev. Cancer* **2008**, *8*, 387−398.

(2) Polakis, P. Wnt Signaling and Cancer. *Genes Dev.* **2000**, *14*, 1837−1851.

(3) Rubinfeld, B.; Souza, B.; Albert, I.; Muller, O.; Chamberlain, S. H.; Masiarz, F. R.; Munemitsu, S.; Polakis, P. Association of the APC Gene Product with Beta-Catenin. *Science* **1993**, *262*, 1731−1734.

(4) Su, L. K.; Vogelstein, B.; Kinzler, K. W. Association of the APC Tumor Suppressor Protein with Catenins. *Science* **1993**, *262*, 1734−1737.

(5) Sato, H.; Suzuki, H.; Toyota, M.; Nojima, M.; Maruyama, R.; Sasaki, S.; Takagi, H.; Sogabe, Y.; Sasaki, Y.; Idogawa, M.; Sonoda, T.; Mori, M.; Imai, K.; Tokino, T.; Shinomura, Y. Frequent Epigenetic Inactivation of DICKKOPF Family Genes in Human Gastrointestinal Tumors. *Carcinogenesis* **2007**, *28*, 2459−2466.

(6) Suzuki, H.; Watkins, D. N.; Jair, K. W.; Schuebel, K. E.; Markowitz, S. D.; Chen, W. D.; Pretlow, T. P.; Yang, B.; Akiyama, Y.; Van Engeland, M.; Toyota, M.; Tokino, T.; Hinoda, Y.; Imai, K.; Herman, J. G.; Baylin, S. B. Epigenetic Inactivation of SFRP Genes Allows Constitutive WNT Signaling in Colorectal Cancer. *Nat. Genet.* **2004**, *36*, 417−422.

(7) Terasaki, H.; Saitoh, T.; Shiokawa, K.; Katoh, M. Frizzled-10, Up-regulated in Primary Colorectal Cancer, Is a Positive Regulator of the WNT - Beta-Catenin - TCF Signaling Pathway. *Int. J. Mol. Med.* **2002**, *9*, 107−112.

(8) Caldwell, G. M.; Jones, C.; Gensberg, K.; Jan, S.; Hardy, R. G.; Byrd, P.; Chughtai, S.; Wallis, Y.; Matthews, G. M.; Morton, D. G. The Wnt Antagonist sFRP1 in Colorectal Tumorigenesis. *Cancer Res.* **2004**, *64*, 883−888.

(9) Okino, K.; Nagai, H.; Hatta, M.; Nagahata, T.; Yoneyama, K.; Ohta, Y.; Jin, E.; Kawanami, O.; Araki, T.; Emi, M. Up-regulation and Overproduction of DVL-1, the Human Counterpart of the Drosophila Dishevelled Gene, in Cervical Squamous Cell Carcinoma. *Oncol. Rep.* **2003**, *10*, 1219−1223.

(10) Polakis, P. Wnt Signaling in Cancer. *Cold Spring Harb. Perspect. Biol.* **2012**, *4*, a008052.

(11) Proffitt, K. D.; Madan, B.; Ke, Z.; Pendharkar, V.; Ding, L.; Lee, M. A.; Hannoush, R. N.; Virshup, D. M. Pharmacological Inhibition of the Wnt Acyltransferase PORCN Prevents Growth of WNT-Driven Mammary Cancer. *Cancer Res.* **2013**, *73*, 502−507.

(12) Coombs, G. S.; Yu, J.; Canning, C. A.; Veltri, C. A.; Covey, T. M.; Cheong, J. K.; Utomo, V.; Banerjee, N.; Zhang, Z. H.; Jadulco, R. C.; Concepcion, G. P.; Bugni, T. S.; Harper, M. K.; Mihalek, I.; Jones, C. M.; Ireland, C. M.; Virshup, D. M. WLS-Dependent Secretion of WNT3A Requires Ser209 Acylation and Vacuolar Acidification. *J. Cell Sci.* **2010**, *123*, 3357−3367.

(13) Takada, R.; Satomi, Y.; Kurata, T.; Ueno, N.; Norioka, S.; Kondoh, H.; Takao, T.; Takada, S. Monounsaturated Fatty Acid Modification of Wnt Protein: Its Role in Wnt Secretion. *Dev. Cell* **2006**, *11*, 791−801.

(14) Rios-Esteves, J.; Haugen, B.; Resh, M. D. Identification of Key Residues and Regions Important for Porcupine-mediated Wnt Acylation. *J. Biol. Chem.* **2014**, *289*, 17009−17019.

(15) Chen, B.; Dodge, M. E.; Tang, W.; Lu, J.; Ma, Z.; Fan, C. W.; Wei, S.; Hao, W.; Kilgore, J.; Williams, N. S.; Roth, M. G.; Amatruda, J. F.; Chen, C.; Lum, L. Small Molecule-Mediated Disruption of Wnt-Dependent Signaling in Tissue Regeneration and Cancer. *Nat. Chem. Biol.* **2009**, *5*, 100−107.

(16) Jiang, X.; Hao, H. X.; Growney, J. D.; Woolfenden, S.; Bottiglio, C.; Ng, N.; Lu, B.; Hsieh, M. H.; Bagdasarian, L.; Meyer, R.; Smith, T. R.; Avello, M.; Charlat, O.; Xie, Y.; Porter, J. A.; Pan, S.; Liu, J.; McLaughlin, M. E.; Cong, F. Inactivating Mutations of RNF43 Confer Wnt Dependency in Pancreatic Ductal Adenocarcinoma. *Proc. Natl. Acad. Sci. U.S.A.* **2013**, *110*, 12649−12654.

(17) Liu, J.; Pan, S.; Hsieh, M. H.; Ng, N.; Sun, F.; Wang, T.; Kasibhatla, S.; Schuller, A. G.; Li, A. G.; Cheng, D.; Li, J.; Tompkins, C.; Pferdekamper, A.; Steffy, A.; Cheng, J.; Kowal, C.; Phung, V.; Guo, G.; Wang, Y.; Graham, M. P.; Flynn, S.; Brenner, J. C.; Li, C.; Villarroel, M. C.; Schultz, P. G.; Wu, X.; McNamara, P.; Sellers, W. R.; Petruzzelli, L.; Boral, A. L.; Seidel, H. M.; McLaughlin, M. E.; Che, J.; Carey, T. E.; Vanasse, G.; Harris, J. L. Targeting Wnt-Driven Cancer through the Inhibition of Porcupine by LGK974. *Proc. Natl. Acad. Sci. U.S.A.* **2013**, *110*, 20224−20229.

(18) Schrödinger. *Maestro, LigPrep, MacroModel, Glide, QikProp & Jaguar*; Schrödinger, LLC: New York, NY, 2012.

(19) Chang, G.; Guida, W. C.; Still, W. C. An Internal-Coordinate Monte Carlo Method for Searching Conformational Space. *J. Am. Chem. Soc.* **1989**, *111*, 4379−4386.

(20) Polak, E. R. Note sur la Convergence de Méthodes de Directions Conjuguées. *Rev. Fr. Inform. Rech. O. Série Rouge* **1969**, *16*, 35−43.

(21) Jorgensen, W. L.; Maxwell, D. S.; Tirado-Rives, J. Development and Testing of the OPLS All-Atom Force Field on Conformational Energetics and Properties of Organic Liquids. *J. Am. Chem. Soc.* **1996**, *118*, 11225−11236.

(22) Kaminski, G. A.; Friesner, R. A.; Tirado-Rives, J.; Jorgensen, W. L. Evaluation and Reparametrization of the OPLS-AA Force Field for Proteins via Comparison with Accurate Quantum Chemical Calculations on Peptides. *J. Phys. Chem. B* **2001**, *105*, 6474−6487.

(23) Halgren, T. A. MMFF VI. MMFF94s Option for Energy Minimization Studies. *J. Comput. Chem.* **1999**, *20*, 720−729.

(24) Hasel, W. H.; T, F.; Still, W. C. A Rapid Approximation to the Solvent Accessible Surface Areas of Atoms. *Tetrahedron Comput. Method.* **1988**, *1*, 103−116.

(25) Still, W. C.; Tempczyk, A.; Hawley, R. C.; Hendrickson, T. Semianalytical Treatment of Solvation for Molecular Mechanics and Dynamics. *J. Am. Chem. Soc.* **1990**, *112*, 6127−6129.

(26) Bostrom, J.; Norrby, P. O.; Liljefors, T. Conformational Energy Penalties of Protein-Bound Ligands. *J. Comput.-Aided Mol. Des.* **1998**, *12*, 383−396.

(27) Tannor, D. J.; Marten, B.; Murphy, R.; Friesner, R. A.; Sitkoff, D.; Nicholls, A.; Honig, B.; Ringnalda, M.; Goddard, W. A. Accurate First Principles Calculation of Molecular Charge Distributions and Solvation Energies from Ab Initio Quantum Mechanics and Continuum Dielectric Theory. *J. Am. Chem. Soc.* **1994**, *116*, 11875−11882.

(28) Duraiswamy, A. J.; Alam, J. WNT Pathway Modulator. PCT/SG2014/000183, 2014.

(29) Ho, S. Y.; Blanchard, S. E.; Duraiswamy, A. J.; Alam, J.; Adsool, V. A. Purine Diones as WNT Pathway Modulators. PCT/SG2014/000217, 2014.

(30) Ho, S. Y.; Alam, J.; Duraiswamy, A. J.; Wang, W. L. WNT Pathway Inhibitors. PCT/SG2014/000602, 2014.

(31) Wang, W. L.; Ho, S. Y.; Alam, J.; Poulsen, A.; Duraiswamy, J. Phthalimide Derivatives as Modulators of WNT Pathway. GB1409783.6, 2014.

DOI: 10.1021/acs.jcim.5b00159
J. Chem. Inf. Model. 2015, 55, 1435−1448

(32) Alam, J.; Poulsen, A.; Ho, S. Y.; Wang, W. L.; Duraiswamy, A. J. Maleimide Derivatives as Modulators of WNT Pathway. PCT/SG2014/000601, 2014.
(33) Cheng, D.; Zhang, G.; Han, D.; Gao, W.; Pan, S. N-(Hetero)aryl,2-(hetero)aryl-Substituted Acetamides for Use as Wnt Signalling Modulators. PCT/US2010/025813, 2010.
(34) Wang, X.; Moon, J.; Dodge, M. E.; Pan, X.; Zhang, L.; Hanson, J. M.; Tuladhar, R.; Ma, Z.; Shi, H.; Williams, N. S.; Amatruda, J. F.; Carroll, T. J.; Lum, L.; Chen, C. The Development of Highly Potent Inhibitors for Porcupine. *J. Med. Chem.* **2013**, *56*, 2700−2704.

DOI: 10.1021/acs.jcim.5b00159
J. Chem. Inf. Model. 2015, 55, 1435−1448